PHYSICAL REVIEW D **87,** 115023 (2013)

Fine tuning in the constrained exceptional supersymmetric standard model

P. Athron,[1,*] Maien Binjonaid,[2,3,†] and S. F. King[2,‡]

[1]*ARC Centre of Excellence for Particle Physics at the Terascale, School of Chemistry and Physics, The University of Adelaide, Adelaide, South Australia 5005, Australia*

[2]*School of Physics and Astronomy, University of Southampton, Southampton SO17 1BJ, United Kingdom*

[3]*Department of Physics and Astronomy, King Saud University, P.O. Box 2455, Riyadh 11451, Saudi Arabia*

(Received 7 March 2013; published 21 June 2013)

Supersymmetric unified models in which the Z' couples to the Higgs doublets, as in the E_6 class of models, have large fine tuning dominated by the experimental mass limit on the Z'. To illustrate this, we investigate the degree of fine tuning throughout the parameter space of the constrained exceptional supersymmetric standard model (cE$_6$SSM) that is consistent with a Higgs mass $m_h \sim 125$ GeV. Fixing $\tan\beta = 10$, and taking specific values of the mass of the Z' boson, with $M_{Z'} \sim 2$–4 TeV, we find that the minimum fine tuning is set predominantly from the mass of Z' and varies from ~200 to 400 as we vary $M_{Z'}$ from ~2 to 4 TeV. However, this is significantly lower than the fine tuning in the constrained minimal supersymmetric standard model, of $\mathcal{O}(1000)$, arising from the large stop masses required to achieve the Higgs mass.

DOI: 10.1103/PhysRevD.87.115023 PACS numbers: 12.60.Jv, 11.30.Pb, 12.60.−i, 14.80.Bn

I. INTRODUCTION

The Large Hadron Collider (LHC) has been accumulating data since 2009 with no observation of new physics beyond the standard model so far, placing strong limits on new colored states in extensions of the standard model. For example, in supersymmetric (SUSY) models there are strong experimental limits on the first- and second-generation squark and gluino masses [1,2], which imply that they must be at least an order of magnitude larger than the electroweak (EW) scale. Within constrained versions of SUSY, where the stop masses are linked to first- and second-generation squark masses, this can considerably increase fine tuning, since the EW scale is very sensitive to stop masses, through the electroweak symmetry-breaking conditions.

At the same time, Atlas and CMS have recently observed a new state consistent with a standard-model-like Higgs boson at $m_h = 125$–126 GeV [3,4], which is within the range for it to be consistent with the lightest Higgs in supersymmetric models. In the minimal supersymmetric standard model (MSSM), this introduces further tension with naturalness, since the light Higgs mass at tree level is bounded from above by the Z boson mass (M_Z). The large radiative contributions from stops needed to raise it to the observed value typically imply very large fine tuning. For example, the constrained MSSM (cMSSM) [5] has been shown to require fine tuning of $\mathcal{O}(1000)$ if it is to contain a 125 GeV Higgs mass [6,7].

Here we consider fine tuning in an alternative class of constrained SUSY models which involves both an extra singlet field, denoted S, and an extra $U(1)$ gauge symmetry at low energy (TeV scale). As the singlet acquires a VEV, denoted s, it produces a μ term, denoted μ_{eff}, and it breaks the extra $U(1)$ gauge symmetry, giving rise to a massive Z' boson. Such models can increase the tree-level physical Higgs boson mass above the M_Z limit of the MSSM, due to both F-term contributions of the singlet and the D-term contributions associated with the Z', allowing lighter stop masses and hence reducing fine tuning due to stop loops. The exceptional supersymmetric standard model (E$_6$SSM) [8,9] is an example of such a model, inspired by the E_6 group. At tree level, the light Higgs mass is given as

$$m_h^2 \approx \underbrace{\underbrace{M_Z^2 \cos^2 2\beta}_{\text{MSSM}} + \frac{\lambda^2}{2} v^2 \sin^2 2\beta}_{\text{NMSSM}} + \underbrace{\frac{M_Z^2}{4}\left(1 + \frac{1}{4}\cos 2\beta\right)^2}_{\text{E}_6\text{SSM}} + \Delta m_h^2, \tag{1}$$

where $\tan\beta = \frac{v_2}{v_1}$ is the ratio between the two Higgs doublets' vacuum expectation values (VEVs), λ is the Yukawa coupling of the singlet field to the Higgs doublets, and Δm_h^2 represents loop corrections.

Indeed, Eq. (1) shows that the E$_6$SSM allows larger tree-level Higgs masses than the NMSSM [10], which in turn allows larger tree-level Higgs masses than the MSSM. This means that the E$_6$SSM does not rely on such a large

*peter.athron@adelaide.edu.au
†mymb1a09@soton.ac.uk, maien@ksu.edu.sa
‡king@soton.ac.uk

 © 2013 American Physical Society

contribution from the radiative correction term Δm_h^2 in order to reproduce the Higgs mass. As a result, the E_6SSM permits lower stop masses than either the NMSSM or the MSSM. In addition, the λ coupling in the E_6SSM can be larger at low energies (while still remaining perturbative all the way up to the GUT scale) than is the case in the NMSSM.

One might conclude that this should lead to lower fine tuning in the E_6SSM than either the NMSSM or MSSM, since the large stop masses are usually the main source of fine tuning in SUSY models. However, the origin of the extra term in Eq. (1) is due to D terms arising from the coupling of the Higgs doublets to the extra $U(1)$ gauge symmetry, and such D terms also contribute to the minimization conditions of the Higgs doublets. Indeed, as we shall discuss, one of the minimization conditions of the E_6SSM can be written in the form

$$c\frac{M_Z^2}{2} = -\mu_{\rm eff}^2 + \frac{(m_d^2 - m_u^2 \tan^2\beta)}{\tan^2\beta - 1} + d\frac{M_{Z'}^2}{2}, \qquad (2)$$

where c, d are functions of $\tan\beta$ which are of order $\sim\mathcal{O}(1)$, m_d^2, m_u^2 are soft Higgs mass-squared parameters and $\mu_{\rm eff}$ arises from the singlet VEV. Written in this form, it is clear that the D terms are a double-edged sword, since they also introduce a new source of tree-level fine tuning, due to the Z' mass-squared term in Eq. (2), which will increase quadratically as $M_{Z'}^2$, eventually coming to dominate the fine tuning for large enough values of $M_{Z'}$. This tree-level fine tuning can be compared to that due to $\mu_{\rm eff}$, which typically requires this parameter to be not much more than 200 GeV, and similar limits also apply to $M_{Z'}$. With the current CMS experimental mass limit for the Z' in the E_6SSM of $M_{Z'} \gtrsim 2.08$ TeV [11], it is clear that there is already a significant, perhaps dominant, amount of fine tuning due to the Z' mass limit.

In this paper we investigate this new and important source of fine tuning, namely that due to the $M_{Z'}$ limit, and compare it to the usual other sources of fine tuning in the framework of the Constrained E_6SSM (cE_6SSM) [12–15]. Although the impact of a SM-like Higgs with $m_h \sim 125$ GeV on the parameters has recently been considered in Refs. [16,17], fine tuning was not considered. In fact, the present study is the first time that fine tuning has been considered in any supersymmetric E_6 model with a low-energy Z'. To obtain the required Higgs mass in the cE_6SSM, it turns out that the SM singlet field, S, must have a VEV $s \geq 5$ TeV, as pointed out in Ref. [16]. This corresponds to a mass of the Z' boson predicted by the model of 1.9 TeV, which almost reaches the experimental bound of 2 TeV [11]. Thus, all the parameter space we study respects the experimental limit on $M_{Z'}$. Fixing $\tan\beta = 10$, and taking specific values of the mass of the Z' boson, $M_{Z'}$, ranging from 1.9 to 3.8 TeV, we find that the current minimum fine tuning in the cE_6SSM, consistent with a Higgs mass $m_h \sim 125$ GeV, varies from $\sim$200 to 400, and is already dominated by the $M_{Z'}$ limit. However, this is significantly lower than the fine tuning in the cMSSM of $\mathcal{O}(1000)$ arising from the large stop masses required to achieve the Higgs mass.

The rest of the paper is organized as follows: Section II provides a short overview of the E_6SSM. Then, the scalar Higgs potential and the electroweak symmetry-breaking (EWSB) conditions are discussed in Sec. III. In Sec. IV we discuss the fine-tuning measure we use, and derive a fine-tuning master formula for the E_6SSM with a brief description of our seminumerical procedure of calculating fine tuning. Section V is where we present our results and discussion, and then we conclude the study in Sec. IV.

II. THE E_6SSM

The exceptional supersymmetric standard model (E_6SSM) is a nonminimal supersymmetric extension of the SM, which provides a low-energy alternative to the MSSM and NMSSM. It is well motivated, both from more fundamental theories due to its connection to E_6 GUTs, heterotic and F-string theory [18], and at the same time as a low-energy effective model, providing solutions to phenomenological problems. For instance, as mentioned in the Introduction, the E_6SSM allows a larger Higgs mass at tree level than in both the MSSM and the NMSSM, thereby requiring smaller contributions from loops. In addition, it also solves the μ problem associated with the MSSM by dynamically producing the μ term at the TeV scale, without introducing the domain walls or tadpole problems that can appear in the NMSSM.

The E_6SSM is based on the Exceptional Lie group E_6. This contains both $SO(10)$ and $SU(5)$ as subgroups,

$$E_6 \to SO(10) \times U(1)_\psi \qquad (3)$$

$$SO(10) \to SU(5) \times U(1)_\chi, \qquad (4)$$

and hence also contains the standard model gauge group, which is a subgroup of $SU(5)$. A linear combination of the two extra $U(1)_\psi$ and $U(1)_\chi$ groups can survive to low energies, where it is spontaneously broken by a SM singlet field, S. This generates the mass of the associated Z' boson and the exotic quarks, as well as dynamically producing a $\mu_{\rm eff}$ term. The model allows right-handed (RH) neutrinos to have Majorana masses at some scale between the GUT and low scales. This is achieved by choosing this linear combination to be

$$U(1)_N = \frac{\sqrt{15}}{4}U(1)_\psi + \frac{1}{4}U(1)_\chi, \qquad (5)$$

such that the RH neutrinos are not charged under $U(1)_N$; hence it is possible to explain the tiny neutrino masses via seesaw mechanisms.

At low energies, the group structure of the model is that of the SM, along with the additional $U(1)_N$ symmetry,

$$E_6 \to SU(5) \times U(1)_N \qquad (6)$$

$$SU(5) \rightarrow SU(3)_c \times SU(2)_w \times U(1)_Y. \quad (7)$$

The matter content of the model is contained in the complete 27-dimensional representation, which decomposes under $SU(5) \times U(1)_N$ to

$$27_i \rightarrow (10, 1)_i + (5^*, 2)_i + (5^*, -3)_i + (5, -2)_i + (1, 5)_i + (1, 0)_i. \quad (8)$$

Ordinary quarks and leptons are contained in the representations (10, 1) and $(5^*, 2)$. The Higgs doublets and exotic quarks are contained in $(5^*, -3)$ and $(5, -2)$. The singlets are contained in (1, 5), and finally the right-handed neutrinos are included in (1, 0).

Moreover, the model requires three 27 representations, hence $i = 1, 2, 3$, in order to ensure anomaly cancellation. This means that there are three copies of each field present in the model. However, only the third generation (by choice) of the two Higgs doublets, and the SM singlet acquire VEVs. The other two generations are called inert. Furthermore, in order to keep gauge coupling unification, non-Higgs fields that come from extra incomplete $27'$, $\bar{27}'$ representations are added to the model. As a result, a μ' term, which is not necessary related to the weak scale, is present in the model.

The full superpotential consistent with the low-energy gauge structure of the E_6SSM contains includes both E_6-invariant terms and E_6-breaking terms, the full details of which are given in Ref. [8]. However, as in the MSSM, it is necessary to forbid proton decay, and therefore a generalization of R parity should be imposed, and additionally, because the E_6SSM includes three generations of every chiral superfield, there needs to be a suppression of new terms which can induce flavor-changing neutral currents. To achieve this, we impose either a Z_2^L symmetry[1] (Model I) or a Z_2^B symmetry[2] (Model II) along with an approximate Z_2^H symmetry, under which all fields are odd except for the third-generation Higgs superfields, which may arise from a family symmetry [19,20].

The Z_2^H-invariant superpotential then reads

$$\begin{aligned} W_{E_6SSM} \approx{}& \lambda_i \hat{S}(\hat{H}_i^d \hat{H}_i^u) + \kappa_i \hat{S}(\hat{D}_i \hat{\bar{D}}_i) + f_{\alpha\beta} \hat{S}_\alpha (\hat{H}_d \hat{H}_\beta^u) \\ &+ \tilde{f}_{\alpha\beta} \hat{S}_\alpha (\hat{H}_\beta^d \hat{H}_u) + \frac{1}{2} M_{ij} \hat{N}_i^c \hat{N}_j^c + \mu'(\hat{H}'\hat{\overline{H}'}) \\ &+ h_{4j}^E (\hat{H}_d \hat{H}') \hat{e}_j^c + h_{4j}^N (\hat{H}_u \hat{H}') \hat{N}_j^c \\ &+ W_{MSSM}(\mu = 0), \end{aligned} \quad (9)$$

where the indices α, $\beta = 1, 2$ and $i = 1, 2, 3$ denote the generations. S is the SM singlet field, H_u, and H_d are the Higgs doublet fields corresponding to the up and down types. Exotic quarks and the additional non-Higgs fields are denoted by D and H', respectively.

Finally, to ensure that only third-generation Higgs-like fields get VEVs, a certain hierarchy between the Yukawa couplings must exist. Defining $\lambda \equiv \lambda_3$, we impose κ_i, $\lambda_i \gg f_{\alpha\beta}$, $\tilde{f}_{\alpha\beta}$, h_{4j}^E, h_{4j}^N. Moreover, we do not impose any unification of the Yukawa couplings at the GUT scale.

III. THE HIGGS POTENTIAL AND THE EWSB CONDITIONS

The scalar Higgs potential is

$$\begin{aligned} V(H_d, H_u, S) ={}& \lambda^2 |S|^2 (|H_d|^2 + |H_u|^2) + \lambda^2 |H_d.Hu|^2 + \frac{g_2^2}{8} (H_d^\dagger \sigma_a H_d + H_u^\dagger \sigma_a H_u)(H_d^\dagger \sigma_a H_d + H_u^\dagger \sigma_a H_u) \\ &+ \frac{g'^2}{8} (|H_d|^2 - |H_u|^2)^2 + \frac{g_1'^2}{2} (Q_1 |H_d|^2 + Q_2 |H_u|^2 + Q_s |S|^2)^2 + m_s^2 |S|^2 + m_d^2 |H_d|^2 \\ &+ m_u^2 |H_u|^2 + [\lambda A_\lambda S H_d.H_u + \text{c.c.}] + \Delta_{\text{Loops}}, \end{aligned} \quad (10)$$

where g_2, $g'(= \sqrt{3/5} g_1)$, and g_1' are the gauge couplings of $SU(2)_L$, $U(1)_Y$ (GUT normalized), and the additional $U(1)_N$, respectively. $Q_1 = -3/\sqrt{40}$, $Q_2 = -2/\sqrt{40}$, and $Q_s = 5/\sqrt{40}$ are effective $U(1)_N$ charges of H_u, H_d and S, respectively. m_s is the mass of the singlet field, and $m_{u,d} \equiv m_{H_{u,d}}$.

The Higgs field and the SM singlet acquire VEVs at the physical minimum of this potential,

$$\langle H_d \rangle = \frac{1}{\sqrt{2}} \begin{pmatrix} v_1 \\ 0 \end{pmatrix}, \quad \langle H_u \rangle = \frac{1}{\sqrt{2}} \begin{pmatrix} 0 \\ v_2 \end{pmatrix}, \quad \langle S \rangle = \frac{s}{\sqrt{2}}, \quad (11)$$

It is reasonable to exploit the fact that $s \gg v$, which will help in simplifying our master formula for fine tuning, as will be seen in Sec. IV. Then, from the minimization conditions,

$$\frac{\partial V_{E_6SSM}}{\partial v_1} = \frac{\partial V_{E_6SSM}}{\partial v_2} = \frac{\partial V_{E_6SSM}}{\partial s} = 0, \quad (12)$$

the EWSB conditions are

$$\begin{aligned} \frac{M_Z^2}{2} = {}& -\frac{1}{2} \lambda^2 s^2 + \frac{(m_d^2 - m_u^2 \tan^2\beta)}{\tan^2\beta - 1} \\ &+ \frac{g_1'^2}{2} (Q_1 v_1^2 + Q_2 v_2^2 + Q_s s^2) \frac{(Q_1 - Q_2 \tan^2\beta)}{\tan^2\beta - 1}, \end{aligned} \quad (13)$$

[1] All superfields except the leptons and survival Higgs are even.

[2] All the exotic quark, lepton and survival Higgs superfields are odd, while all the other superfields remain even.

$$\sin 2\beta \approx \frac{\sqrt{2}\lambda A_\lambda s}{m_d^2 + m_u^2 + \lambda^2 s^2 + \frac{g_1'^2}{2} Q_s s^2 (Q_1 + Q_2)}, \quad (14)$$

$$m_s^2 \approx -\frac{1}{2} g_1'^2 Q_s^2 s^2 = -\frac{1}{2} M_{Z'}^2, \quad (15)$$

where $M_Z^2 = \frac{1}{4}(g'^2 + g_2^2)(v_2^2 + v_1^2)$ and $M_{Z'}^2 \approx g_1'^2 Q_s^2 s^2$.

Equation (13) can be written in the form

$$c\frac{M_Z^2}{2} = -\mu_{\text{eff}}^2 + \frac{(m_d^2 - m_u^2 \tan^2\beta)}{\tan^2\beta - 1} + d\frac{M_{Z'}^2}{2}, \quad (16)$$

where c, d are functions of $\tan\beta$ which are of order $\sim\mathcal{O}(1)$ and we have written $\mu_{\text{eff}} = \frac{\lambda s}{\sqrt{2}}$. Written in this form, it is clear that fine tuning will increase as $M_{Z'}$ increases. Another source of fine tuning is the large $|\mu_{\text{eff}}|$ term as mentioned in the Introduction, since satisfying Eq. (16) will require this term to compensate for any increase in either the second term (term 2: $\sim m_u^2$, m_d^2) or the last term (term 3: $\sim M_{Z'}^2$).

The increasing experimental limits on $M_{Z'}(\sim s)$ result in constraining the parameter space of the E_6SSM such that only relatively large values of m_0 and $m_{1/2}$ result in successful solutions to the EWSB conditions (Figs. 1–11).

Moreover, imposing universal boundary conditions, which is what characterizes the cE$_6$SSM, means that all low-energy SUSY parameters can be expanded in terms of a few GUT-scale universal and fundamental input parameters, namely

$$m_0, \quad m_{1/2}, \quad A, \quad \lambda_i(0), \quad \kappa_i(0), \quad h_{t,b,\tau}(0), \quad (17)$$

where, m_0, $m_{1/2}$, and A are a universal scalar mass, a universal gaugino mass, and a universal trilinear coupling,

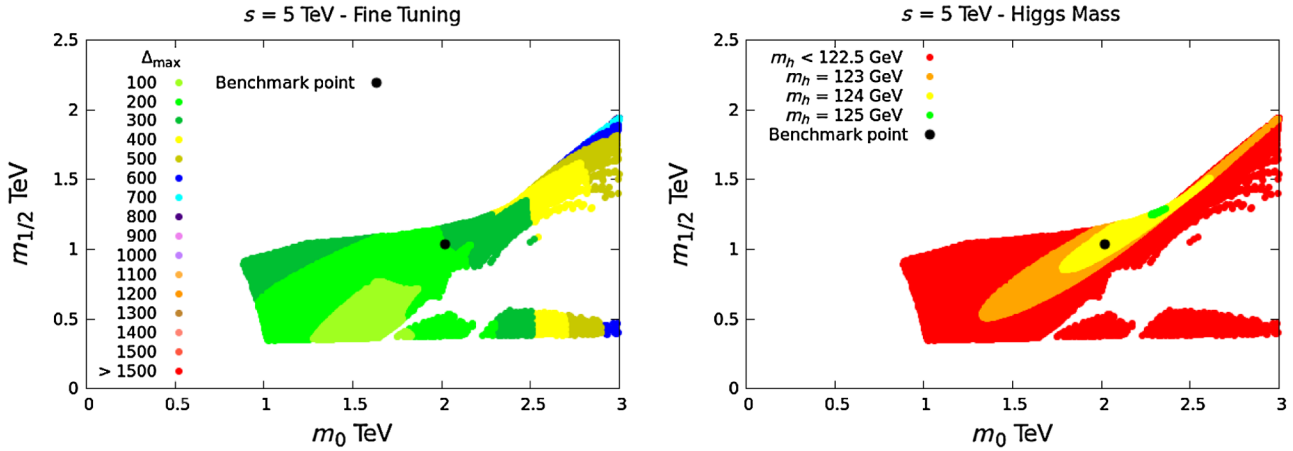

FIG. 1 (color online). Δ_{max} (left) and m_h (right) in the m_0-$m_{1/2}$ plane for $\tan\beta = 10$ and $s = 5$ TeV corresponding to $M_{Z'} = 1.9$ TeV. We also fixed $\lambda_{1,2}(0) = 0.1$ while scanning over $-3 \leq \lambda_3(0) \leq 0$ and $0 \leq \kappa_{1,2,3}(0) \leq 3$. The benchmark point corresponds to $m_0 = 2020$, $m_{1/2} = 1033$ GeV.

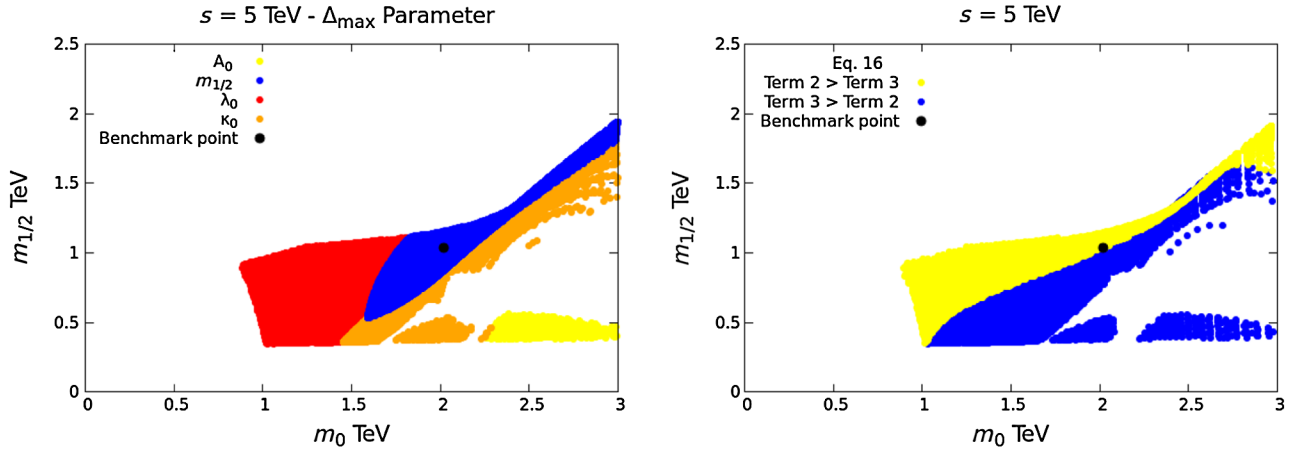

FIG. 2 (color online). The left panel highlights the parameter responsible for the largest amount of fine tuning, Δ_{max}, in the m_0-$m_{1/2}$ plane for $\tan\beta = 10$ and $s = 5$ TeV corresponding to $M_{Z'} = 1.9$ TeV. On the right, a coarse scan shows which terms in Eq. (16) give the largest contribution, with regions where the largest contribution comes from term 2, which is proportional to $m_d^2 - m_u^2 \tan^2\beta$, shown in yellow; and regions where the dominant contribution is from term 3, proportional to $M_{Z'}^2$, shown in blue.

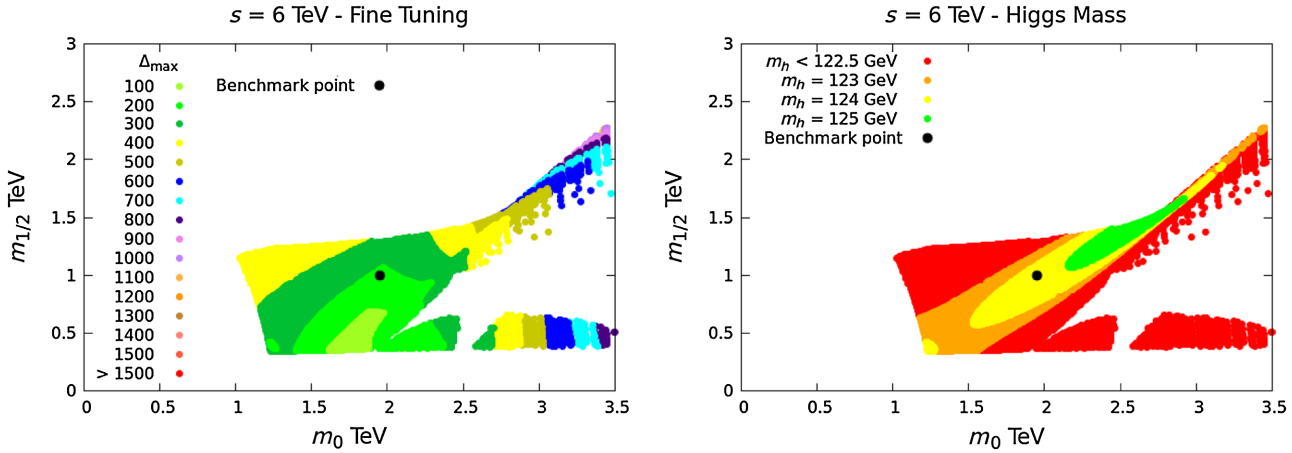

FIG. 3 (color online). $\Delta_{\max}$ (left) and m_h (right) in the m_0-$m_{1/2}$ plane for $\tan\beta = 10$ and $s = 6$ TeV corresponding to $M_{Z'} = 2.3$ TeV. The benchmark point corresponds to $m_0 = 1951$, $m_{1/2} = 1003$ GeV.

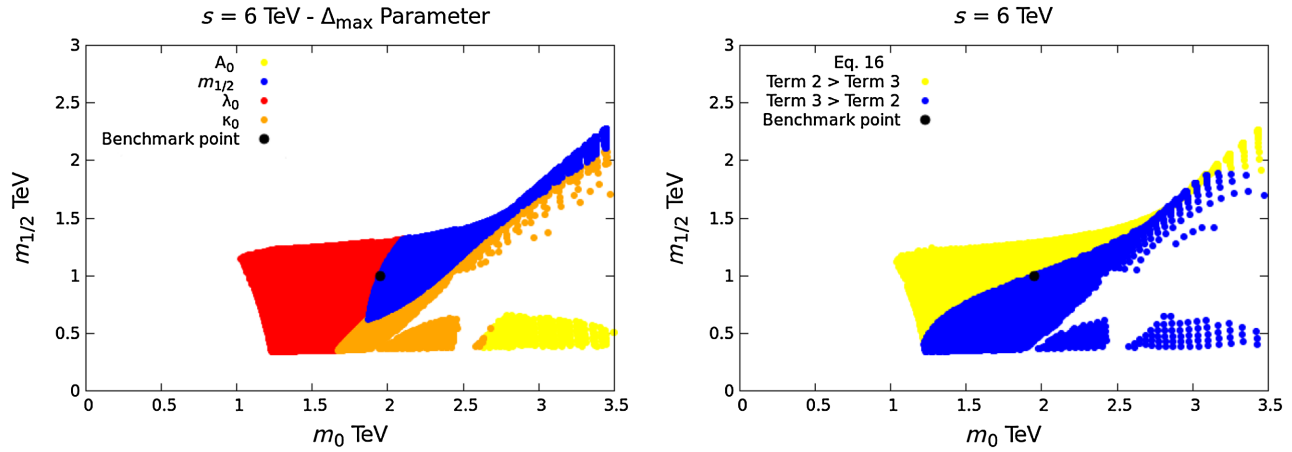

FIG. 4 (color online). The left panel highlights the parameter responsible for the largest amount of fine tuning, $\Delta_{\max}$, in the m_0-$m_{1/2}$ plane for $\tan\beta = 10$ and $s = 6$ TeV corresponding to $M_{Z'} = 2.3$ TeV. On the right, a coarse scan shows which terms in Eq. (16) give the largest contribution, with regions where the largest contribution comes from term 2, which is proportional to $m_d^2 - m_u^2 \tan^2\beta$, shown in yellow; and regions where the dominant contribution is from term 3, proportional to $M_{Z'}^2$, shown in blue.

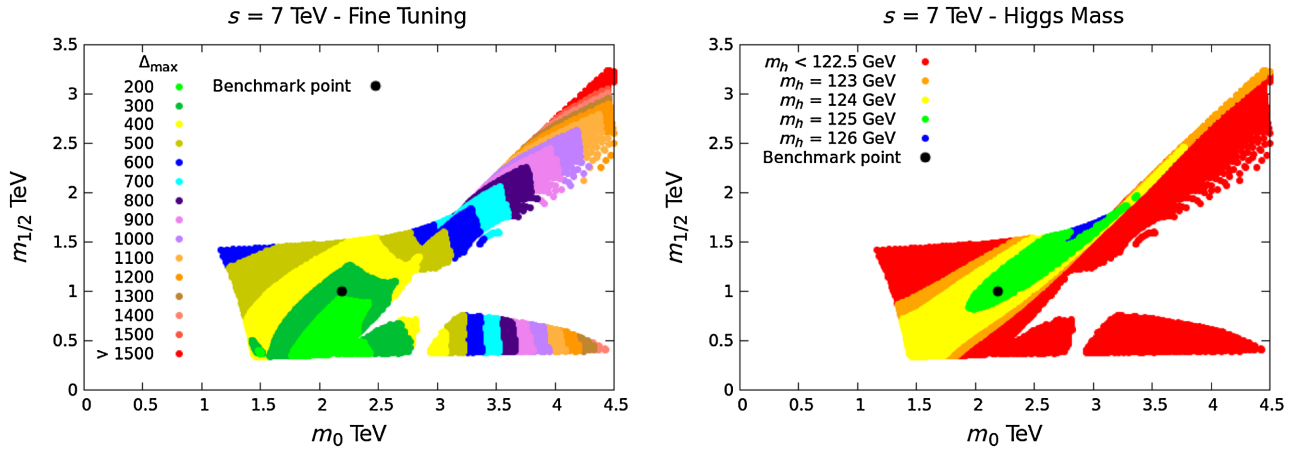

FIG. 5 (color online). $\Delta_{\max}$ (left) and m_h (right) in the m_0-$m_{1/2}$ plane for $\tan\beta = 10$ and $s = 7$ TeV corresponding to $M_{Z'} = 2.6$ TeV. The benchmark point corresponds to $m_0 = 2186$, $m_{1/2} = 1004$ GeV.

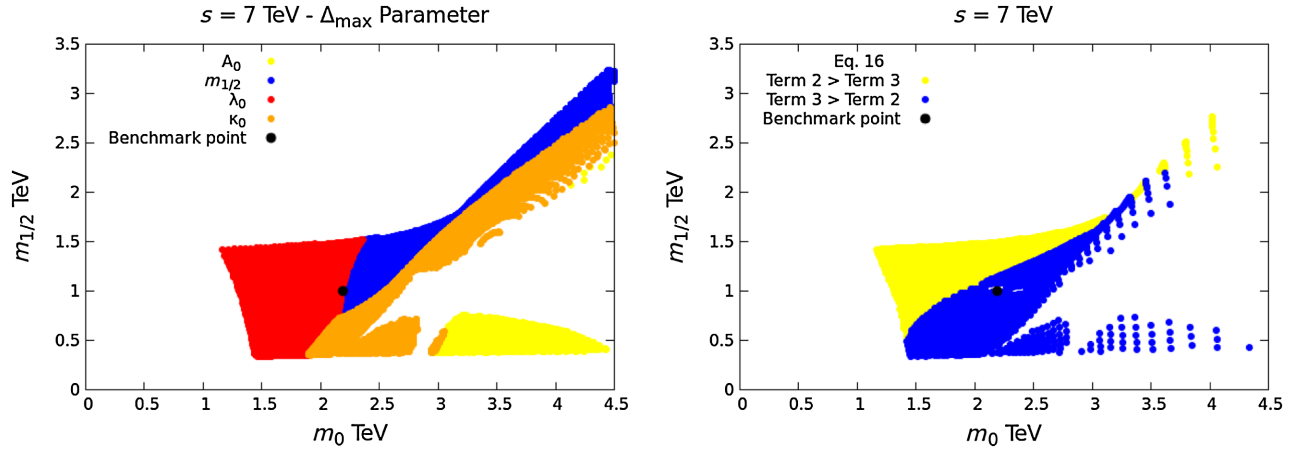

FIG. 6 (color online). The left panel highlights the parameter responsible for the largest amount of fine tuning, $\Delta_{\max}$, in the m_0-$m_{1/2}$ plane for $\tan\beta = 10$ and $s = 7$ TeV corresponding to $M_{Z'} = 2.6$ TeV. On the right, a coarse scan shows which terms in Eq. (16) give the largest contribution, with regions where the largest contribution comes from term 2, which is proportional to $m_d^2 - m_u^2 \tan^2\beta$, shown in yellow; and regions where the dominant contribution is from term 3, proportional to $M_{Z'}^2$, shown in blue.

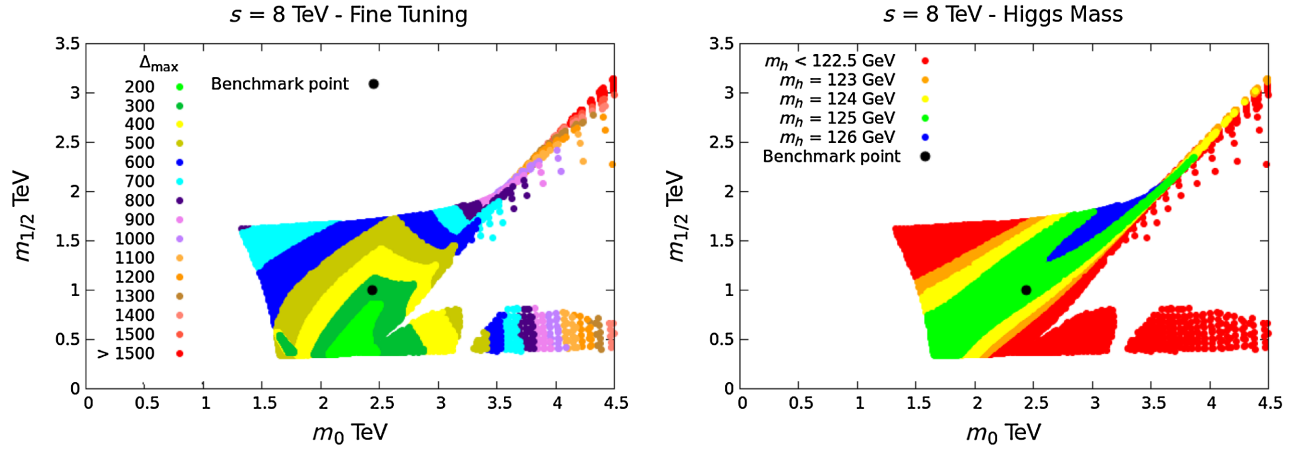

FIG. 7 (color online). $\Delta_{\max}$ (left) and m_h (right) in the m_0-$m_{1/2}$ plane for $\tan\beta = 10$ and $s = 8$ TeV corresponding to $M_{Z'} = 3.0$ TeV. The benchmark point corresponds to $m_0 = 2441$, $m_{1/2} = 1002$ GeV.

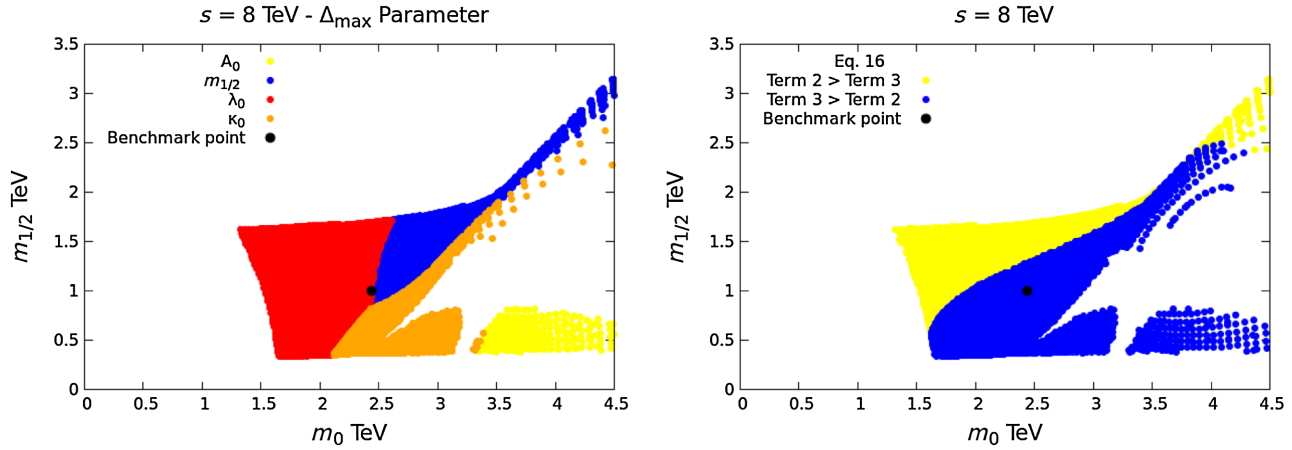

FIG. 8 (color online). The left panel highlights the parameter responsible for the largest amount of fine tuning, $\Delta_{\max}$, in the m_0-$m_{1/2}$ plane for $\tan\beta = 10$ and $s = 8$ TeV corresponding to $M_{Z'} = 3.0$ TeV. On the right, a coarse scan shows which terms in Eq. (16) give the largest contribution, with regions where the largest contribution comes from term 2, which is proportional to $m_d^2 - m_u^2 \tan^2\beta$, shown in yellow; and regions where the dominant contribution is from term 3, proportional to $M_{Z'}^2$, shown in blue.

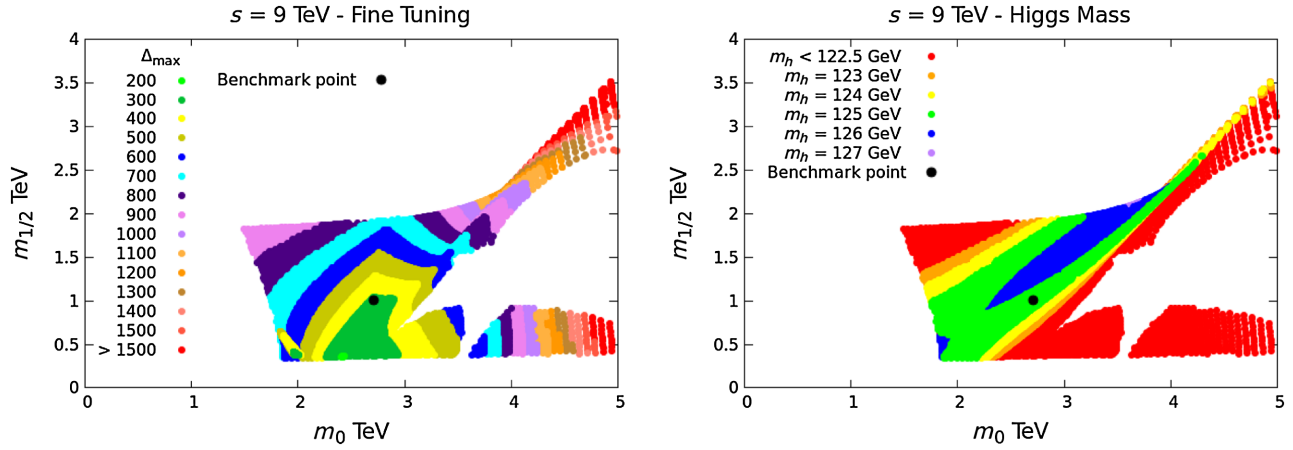

FIG. 9 (color online). $\Delta_{\max}$ (left) and m_h (right) in the m_0-$m_{1/2}$ plane for $\tan\beta = 10$ and $s = 9$ TeV corresponding to $M_{Z'} = 3.4$ TeV. The benchmark point corresponds to $m_0 = 2709$, $m_{1/2} = 1001$ GeV.

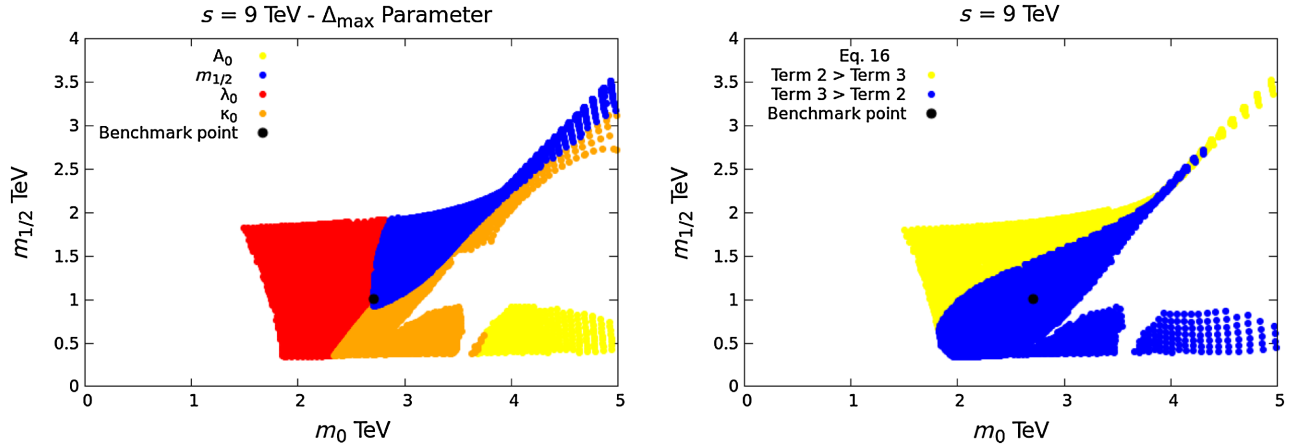

FIG. 10 (color online). The left panel highlights the parameter responsible for the largest amount of fine tuning, $\Delta_{\max}$, in the m_0-$m_{1/2}$ plane for $\tan\beta = 10$ and $s = 9$ TeV corresponding to $M_{Z'} = 3.4$ TeV. On the right, a coarse scan shows which terms in Eq. (16) give the largest contribution, with regions where the largest contribution comes from term 2, which is proportional to $m_d^2 - m_u^2 \tan^2\beta$, shown in yellow; and regions where the dominant contribution is from term 3, proportional to $M_{Z'}^2$, shown in blue.

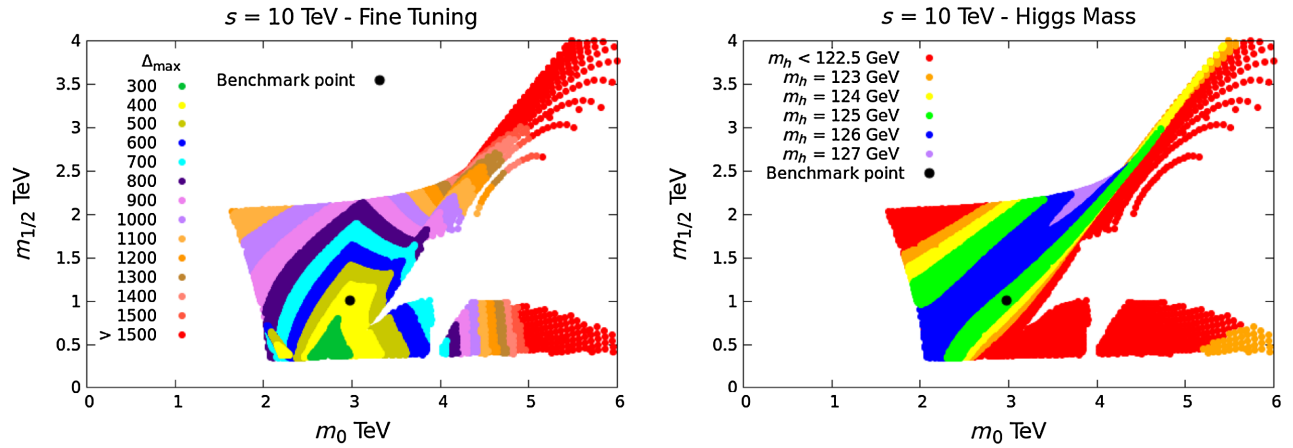

FIG. 11 (color online). $\Delta_{\max}$ (left) and m_h (right) in the m_0-$m_{1/2}$ plane for $\tan\beta = 10$ and $s = 10$ TeV corresponding to $M_{Z'} = 3.8$ TeV. The benchmark point corresponds to $m_0 = 2975$, $m_{1/2} = 1005$ GeV.

respectively, and (0) means taking the parameter at the GUT scale [in the Results section, we refer to $\lambda_3(0)$ and $\kappa_{1,2,3}(0)$ as λ_0 and κ_0, respectively].

This is accomplished by using the one-loop renormalization group equations of the scalar masses, so that one can express $m^2_{H_u}$ at the SUSY scale, M_S, as

$$m^2_{H_u}(M_S) = z_1 m_0^2 + z_2 m_{1/2}^2 + z_3 A^2 + z_4 m_{1/2} A. \quad (18)$$

Then it is possible to write

$$\frac{M_Z^2}{2} \approx \sum_{i=1}^{n} F_i z_i a_i^2, \quad (19)$$

where a denotes the fundamental parameters, and z is the coefficient corresponding to each parameter and is calculated numerically. F is some factor, possibly involving $\tan\beta$.

Whence one can calculate (analytically or numerically) the sensitivity of M_Z to each fundamental parameter, this leads us to fine tuning.

IV. FINE TUNING AND THE MASTER FORMULA

To study the degree of fine tuning, a quantitative measure needs to be applied. Here we use the conventional fine-tuning measure [21,22], where the fractional change in the observable is calculated for a given fractional change in the input parameter,

$$\Delta_a = \left| \frac{\partial \ln M_Z}{\partial \ln a} \right|, \quad (20)$$

where M_Z is the mass of the Z boson[3] and a is one of the fundamental parameters in the set $\{m_0, m_{1/2}, A, \lambda(0), \kappa(0)\}$.

For example, $\Delta_a = 10$ and 200 correspond to a 10% and 0.5% tuning in the parameter a, respectively. Moreover, for a given point in the parameter space, fine tuning is the maximum value of fine tuning in the set $\{\Delta_a\}$, and is denoted $\Delta_{\max}$ (or simply Δ).

This measure has been used extensively within the literature, e.g. Refs. [23–45].

A. Alternative tuning measures

Some concerns have been raised in the literature regarding the use of this measure, and its use is not universal, with a number of alternative measures having been introduced and applied [46–60]. The $\{\Delta_a\}$ measure the sensitivity of the parameters to the observable, and as such are very dependent on the parametrization chosen. In particular, whether one takes p_i to be the parameter or instead chooses $a = p_i^2$ introduces a factor-2 difference, and this factor of 2 will then appear for every point in the parameter space. To remove this *global sensitivity* one can choose some normalization [46–49] on the Δ_a; however, this then introduces questions about the bounds on the parameters, and the probability is not clearly defined or understood.

Additionally, the overall tuning is chosen by taking Δ as the maximum of the individual sensitivities $\{\Delta_a\}$, but a proposed alternative is to combine them in quadrature, like uncorrelated errors [54–57]. Clearly these measures can differ substantially, but it is not obvious which should be chosen. A new measure [59] defined tuning[4] as the ratio of the parameter space volume (defined by fixed dimensionless variations in the parameters) to the same volume with the additional constraint that the dimensional variations of the observable are no greater than those of the parameters. As such, this measure automatically combined the tuning from each parameter into a single tuning defined in terms of parameter-space volume. For the simple cases studied, it was shown that this new measure was in greater agreement with the conventional measure than the alternative where the sensitivities are combined in quadrature, which might be understood as being due to large correlations between the individual sensitivities.

Finally, all the measures described so far define tuning as a theoretical feature of a point in parameter space, measuring how natural a point is. As such, these measures quantify how natural phenomenologically acceptable points are once experimental limits have ruled out points which were initially favored as being natural (or more natural). Instead, within Bayesian analyses natural expectations for parameter space points, given by the prior distribution, are combined with experimental data to determine the probability defined as a degree of belief. If one must fine-tune the parameters to get the measured values of observables correct, then this will correspond to only a tiny fraction of the total integrated prior volume, and therefore fine-tuned scenarios should be automatically penalized. However, in practice, in MSSM studies M_Z is often fixed to its experimental value at the outset, reducing the dimensionality of the parameter space and missing the fine tuning. To fix this, one can start off with a full set of parameters with the chosen prior distribution, unconstrained by EWSB requirements and then perform a Jacobian transformation [7,61–65]. The Jacobian factor accounts for the missed fine tuning and introduces similar derivatives to those appearing in the sensitivity criterion, so it then appears as an effective "fine-tuning prior."

In the MSSM, the conventional measure of fine tuning is numerically very close to this effective fine-tuning prior (see e.g. Ref. [7]) and has sometimes been used directly as

[3]Note that some authors choose M_Z^2 instead of M_Z. Both measures can be easily linked, since $\frac{1}{2}\Delta_a(M_Z^2) = \Delta_a(M_Z)$. Our choice was made to enable straightforward comparisons with the results in Ref. [7].

[4]This measure also allows one to combine several observables and has a normalized version of the tuning measure to deal with global sensitivity in a similar manner to Refs. [46–49], but with a slightly different normalization and interpretation in terms of probabilities.

a fine-tuning prior [32,66], without directly calculating the Jacobian factor.

Nonetheless, the conventional tuning remains a very simple and useful measure and has continued to be used widely with the literature. We will employ it here for the following reasons:

(1) It is the most widely used tuning measure with which one can compare.
(2) It gives a good approximation of the effective fine-tuning prior.
(3) It is simple to understand and apply.
(4) It provides a better match to the more complicated multiparameter measure [59] than combining sensitivities in quadrature.

In particular, please note that the simplicity and wide use is very important, since this is the first quantitative investigation into tuning in this model, and therefore comparison to what has been done in other models is of greater significance. Applying this measure provides a quantification of the severity of tuning in the model, and shows which regions have the least fine tuning and could be used as an "effective fine-tuning prior" in future Bayesian studies of the model.

B. Master formula

Having concluded the discussion on the motivation and suitability of this measure, we now proceed to apply it in a quantitative analysis of fine tuning. To do so, we first derive and present the master formula which gives the explicit expression from which the fine tuning is calculated. Using Eqs. (13)–(15) and (20), we derive this master formula[5] for fine tuning in the E_6SSM:

$$\Delta_a \approx c^{-1} \times \frac{a}{M_Z^2(\tan^2\beta - 1)} \Bigg\{ \frac{(1-\tan^2\beta)}{2} \frac{\partial(\lambda^2 s^2)}{\partial a} + \frac{\partial m_d^2}{\partial a} - \tan^2\beta \frac{\partial m_u^2}{\partial a} + \frac{g_1'^2}{2}(Q_1 - \tan^2\beta Q_2) \times \left(Q_s \frac{\partial s^2}{\partial a} + \frac{4M_Z^2}{\bar{g}^2} \frac{\partial}{\partial a}(Q_1 \cos^2\beta + Q_2 \sin^2\beta) \right) - \frac{\tan\beta}{\cos 2\beta} \left[1 + \frac{M_Z^2}{m_d^2 + m_u^2 + \lambda^2 s^2 + \frac{g_1'^2}{2} Q_s s^2 (Q_1 + Q_2)} \right] \times \left[\sqrt{2} \frac{\partial(\lambda A_\lambda s)}{\partial a} - \sin 2\beta \frac{\partial}{\partial a} \left(m_d^2 + m_u^2 + \lambda^2 s^2 + \frac{g_1'^2}{2} Q_s (Q_1 + Q_2) s^2 \right) \right] \Bigg\}, \tag{21}$$

where

$$c = \left[1 - \frac{4}{(\tan^2\beta - 1)} \frac{g_1'^2}{\bar{g}^2} (Q_1 - \tan^2\beta Q_2) \times (Q_1 \cos^2\beta + Q_2 \sin^2\beta) \right] \tag{22}$$

and $\bar{g}^2 = (g'^2 + g_2^2)$. For $\tan\beta = 10$, $c^{-1} \simeq 0.88$.

The aim is to expand the low-energy parameters, including s, in terms of the GUT-scale universal input parameters using the E_6SSM renormalization group equations as mentioned in the previous section. Next, the formula is implemented into a private cE$_6$SSM spectrum generator (described in Refs. [14,15]), and fine tuning at each point in the scanned parameter space is calculated. In order to ensure accuracy of the results, the derivatives in the master formula for $a = \lambda(0)$ and $a = \kappa(0)$ are calculated numerically. And in order to calculate

$$\frac{\partial}{\partial a} s^2, \tag{23}$$

we use

$$s^2 = -\frac{2}{g_1'^2 Q_s^2} m_s^2, \tag{24}$$

where, as usual, m_s^2 is expanded in terms of the GUT parameters.

Finally, throughout our study, we fix $\tan\beta = 10$, since larger and smaller values restrict the availability of $m_h \sim 125$ GeV and the parameter space [16].

V. RESULTS AND DISCUSSION

The scans are taken for fixed $s = 5$–10 TeV corresponding to $M_{Z'} = 1.9$–3.8 TeV. We scan over

$$-3 \lesssim \lambda_3(0) \lesssim 0 \quad \text{and} \quad 0 \lesssim \kappa_1(0) = \kappa_2(0) = \kappa_3(0) \lesssim 3 \tag{25}$$

while fixing $\lambda_{1,2}(0) = 0.1$ and $\tan\beta = 10$. The sign of $\lambda \equiv \lambda_3(0)$ is a free parameter in our convention since we are setting s and $m_{1/2} > 0$. However, as with previous studies [16], we found that most of the parameter space is covered with $\lambda < 0$, while $\lambda > 0$ covers a much smaller region of the parameter space. Therefore, we focused on $\lambda < 0$ in our study. The other GUT parameters—m_0, $m_{1/2}$ and A_0—are obtained as an output so that the EWSB conditions are satisfied to one-loop order. Then we plot both m_h and $\Delta_{\max}$ in the m_0-$m_{1/2}$ plane. The key at the top-left of all plots corresponding to m_h shows the central value

[5] Note that we have left two terms in the second line of Eq. (21) written in terms of derivatives of $\cos^2\beta$ and $\sin^2\beta$ with respect to a. Substituting for soft masses here would unnecessarily clutter the expression, and we note that these terms are numerically negligible since their contribution to fine tuning is very small [$< \mathcal{O}(1)$]. This is due to the fact that they will be multiplied by an overall factor of order $\mathcal{O}(<10^{-12})$.

in a bin of width ± 0.5 GeV, while that corresponding to Δ shows the central value in a bin of width ± 50.

Moreover, we select a benchmark point corresponding to each value of s. These points possess the smallest fine tuning in the m_0-$m_{1/2}$ plane consistent with a Higgs mass within the $124 < m_h < 127$ GeV range, and $m_{\tilde{g}} \geq 850$ GeV. They are denoted with a black dot in Figs. 1–12. These points and the relevant physical masses are summarized in Table I in Appendix A

In the left panel of Fig. 1, the results for $s = 5$ TeV, corresponding to $M_{Z'} = 1.9$ TeV, are shown with fine-tuning contours, ranging from 100 to above 800 for the highest m_0. For each value of m_0 and $m_{1/2}$, the parameters λ, κ, and A take different values. Since the Higgs mass strongly depends both on stop corrections and on λ, it will also take different values denoted by the Higgs mass contours displayed in the right panel of Fig. 1. Since both fine tuning and the Higgs mass vary over the m_0-$m_{1/2}$ plane, the mass of the Higgs discovered at the LHC plays a crucial rule in fixing the level of tuning, though this dependence is significantly more complicated than in the MSSM. Thus, although for $s = 5$ TeV the tuning can in principle be as low as 100, in order to obtain $m_h \sim 124$ GeV the fine tuning must be more than twice as large as this. A benchmark representing points with the lowest tuning compatible with data is shown as black dots in Fig. 1 having $\Delta_{\rm BM} = 251$ with $m_h \approx 124$ GeV. Note that $m_h \sim 125$ GeV is almost impossible to achieve for $s = 5$ TeV (represented by the very small green region in the right panel). In addition, the value $M_{Z'} = 1.9$ TeV slightly violates the CMS limit $M_{Z'} \gtrsim 2.08$ TeV [11], although this limit does not take into account the presence of lighter singlet states which increase the Z' width and reduce the leptonic branching ratio, weakening this limit as discussed in Ref. [12].

One also needs to take into account LHC constraints from squark and gluino searches, which rule out $m_{1/2} \lesssim 1$ TeV corresponding to a gluino mass $m_{\tilde{g}} \lesssim 850$ GeV [16].

In Appendix A we provide a set of benchmark points corresponding to $m_{1/2} \sim 1$ TeV, and these benchmark points are denoted by small black dots on the figures. We emphasize that the cE$_6$SSM has not been studied by any of the LHC experiments, and that the gluino mass limits in the E$_6$SSM may differ from those of the MSSM as discussed recently [67]. Therefore, in choosing our minimum tuning benchmarks, the limits we assumed are quite conservative. From the results in Ref. [16], we find that in the cE$_6$SSM, the gluino mass is approximately given by $m_{\tilde{g}} \sim 0.85 m_{1/2}$ and the first- and second-generation squark masses are given by $m_{\tilde{q}} \sim (1.3\text{–}1.8) m_0$, depending on $m_{1/2}$. In the future (for example, when the full 8 TeV data set is analyzed), the allowed values of m_0 and $m_{1/2}$ are expected to increase according to these approximate relations. Therefore, we show in Appendix B (Table II) the minimum allowed fine tuning associated with gluino mass in the $1 \leq m_{\tilde{g}} \leq 1.5$ TeV range, and the usual range for the singlet VEV $s = 5$–10 TeV. Clearly, the fine tuning in the cE$_6$SSM is not as large as that in the CMSSM, where increasing $m_{\tilde{g}}$ to 1.5 TeV leads to minimum fine tuning > 1000 as found in Ref. [7], while it varies between $\sim$600 and 800 the cE$_6$SSM.

At first sight, the distribution of fine tuning in the m_0-$m_{1/2}$ plane could seem counterintuitive, since one might expect the region of smaller values of m_0 and $m_{1/2}$ to possess lower fine tuning. However, the variation of $\Delta_{\rm max}$ can be understood by studying which parameter contributes the maximum fine tuning at each point in the parameter space. We show this in Fig. 2 (left panel), where it is clear that the region of small m_0 and $m_{1/2}$ is dominated by large fine tuning in the parameter λ_0, resulting from a large $|\mu_{\rm eff}|$ term in this region.

In addition, κ_0 can contribute to $\Delta_{\rm max}$, since A_λ and m_s are strongly dependent on this parameter. The physical origin of the fine tuning in κ_0 is due to the loops of exotic D particles which serve to radiatively drive the singlet mass squared negative, which triggers electroweak symmetry breaking. Finally, m_0 can be the source of fine tuning for very large values of m_0, which is the region extending beyond what we show in the plots.

The relative fine tuning in the input parameters $\{m_0, m_{1/2}, A, \lambda(0), \kappa(0)\}$ does not directly tell us any information about the relative importance of the second and third terms on the right-hand side of Eq. (16), both of which can independently be large and hence lead to a large $|\mu_{\rm eff}|$ which is manifested as large fine tuning in λ_0. It is therefore instructive to directly compare the magnitudes of the second and third terms of Eq. (16), where the former is proportional to m_u^2 and m_d^2, hence sfermions, and the latter is proportional to $M_{Z'}^2$. In Fig. 2 (right panel), we scan the parameter space for $s = 5$ TeV, and for each point we show which of the two terms is larger. The larger of the two would be responsible for the fine tuning at the corresponding point. It is clear, then, that $M_{Z'}$ (blue region) not only controls the minimum fine tuning allowed, but also is the dominating source of fine tuning over large regions of the parameter space. This is true for all the other values of s. However, some substantial contribution to fine tuning comes from sfermions as seen in the yellow region.

As we increase s to 6 TeV (shown in Fig. 3), we simultaneously satisfy the CMS mass limit on the Z' mass, with $M_{Z'} = 2.3$ TeV, and we obtain more points with the heavier Higgs mass $m_h = 125$ GeV. Interestingly, the benchmark point in this case has a fine tuning $\Delta_{\rm BM} = 233$ for $m_h \approx 124$ GeV, which is slightly smaller than for the previous case with $s = 5$ TeV. Additionally, in the left panel in Fig. 3, a tiny region of $\Delta_{\rm max} = 200$ appears as a small circle inside the $\Delta_{\rm max} = 300$ band. While it is still λ_0 that is responsible for $\Delta_{\rm max}$ in that area as seen in the left panel in Fig. 4, this region is

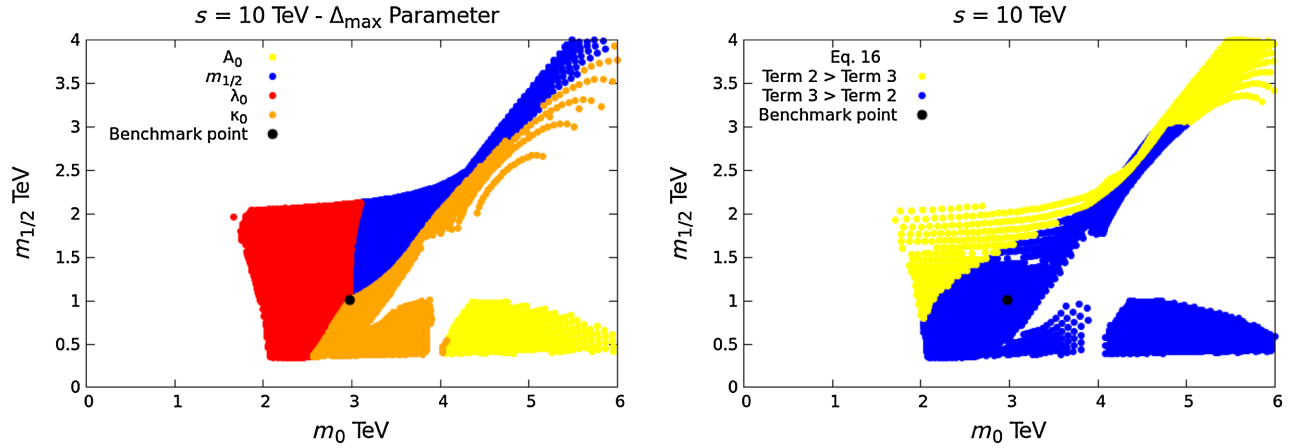

FIG. 12 (color online). The left panel highlights the parameter responsible for the largest amount of fine tuning, $\Delta_{\max}$, in the m_0-$m_{1/2}$ plane for $\tan\beta = 10$ and $s = 10$ TeV corresponding to $M_{Z'} = 3.8$ TeV. On the right, a coarse scan shows which terms in Eq. (16) give the largest contribution, with regions where the largest contribution comes from term 2, which is proportional to $m_d^2 - m_u^2 \tan^2\beta$, shown in yellow; and regions where the dominant contribution is from term 3, proportional to $M_{Z'}^2$, shown in blue.

associated with a slightly smaller $|\mu_{\text{eff}}|$ ($|\lambda_0|$) and larger κ_0 than in the adjacent regions, an effect which was not present in the results of $s = 5$ TeV.

Moreover, Fig. 4 shows that the origin of fine tuning depends on the point in the m_0-$m_{1/2}$ plane consistent with the Higgs mass and the LHC limits of squark and gluino masses, estimated above as $m_{\tilde{g}} \sim 0.85 m_{1/2}$ and $m_{\tilde{q}} \sim (1.3\text{–}1.8) m_0$. For example, if the squark and gluino masses are increased, then it is possible that fine tuning is dominated by fine tuning in $m_{1/2}$ or in λ_0 via large $|\mu_{\text{eff}}|$, which could be due to heavy stop masses rather than large $M_{Z'}$ according to the right panel in Fig. 4.

For $s = 7$ TeV, corresponding to $M_{Z'} = 2.6$ TeV, the region with $m_h \sim 125$ GeV expands in comparison to $s = 5$ and 6 TeV, as can be seen by comparing the right panel in Fig. 5 to the previous plots. In addition, a very small region with $m_h \sim 126$ GeV appears for the first time. In the left panel of Fig. 5, fine tuning starts from 200 and reaches 600 outside the middle region. In addition, the tiny circle of points with smaller fine tuning than its surroundings in the small m_0-$m_{1/2}$ region, which appeared previously in the results for $s = 6$ TeV, now grows a little.

The chosen benchmark point has $\Delta_{\text{BM}} = 270$ for $m_h \approx 125$ GeV. Notice how increasing s, hence $M_{Z'}$, affects the lowest fine tuning possible in the parameter space, confirming that it is the $M_{Z'}$ term in Eq. (16) dominating fine tuning and defining its lowest value, as can be seen in the right panel of Fig. 6. As before, this conclusion depends on the particular point in the m_0-$m_{1/2}$ plane.

For $s = 8$ TeV, the Higgs mass $m_h \sim 125$ GeV dominates over most of the m_0-$m_{1/2}$ plane, as shown in the right panel of Fig. 7. Also, the $m_h \sim 126$ GeV region has become larger. However, fine tuning starts from 300, and the portion of the parameter space with $\Delta_{\max} \geq 500$ is now more apparent than in the $s = 7$ TeV case. The benchmark point has $\Delta_{\text{BM}} = 302$ for $m_h \approx 125$ GeV. The dominance of the $M_{Z'}$ term in Eq. (16) for fine tuning can be seen in the right panel of Fig. 8, with this conclusion dependent on the particular point in the m_0-$m_{1/2}$ plane.

As we reach $s = 9$ TeV, corresponding to $M_{Z'} = 3.4$ TeV, which is shown in Fig. 9, we see that the region where $m_h \sim 125$ GeV starts to shrink and is replaced by $m_h \sim 126$ GeV. If the Higgs mass is indeed $m_h \sim 126$ GeV, then there is a preference for $s = 9$ TeV, especially for smaller values of m_0 and $m_{1/2}$. This illustrates the importance of an accurate determination in the Higgs mass for selecting the most appropriate value of s. Fine tuning starts from 200, although a very small region, and quickly increases to 500 such that a significant portion of the parameter has $\Delta_{\max} \gtrsim 500$. The benchmark point has $\Delta_{\text{BM}} = 330$ for $m_h \approx 125$ GeV. The dominance of the $M_{Z'}$ term in Eq. (16) for fine tuning can be seen in the right panel of Fig. 10, as usual dependent on the particular point in the m_0-$m_{1/2}$ plane.

Finally, for $s = 10$ TeV, corresponding to $M_{Z'} = 3.4$ TeV, in the left panel of Fig. 11, the fine tuning starts from 300, and the parameter space is severely restricted in terms of fine tuning, as it is mostly covered by points with $\Delta_{\max} > 500$. In addition, the region of $m_h \sim 125$ GeV has shrunk and now occupies a smaller portion than the $m_h \sim 126$ GeV region. In addition, a small region with $m_h \sim 127$ GeV now exists prominently for the first time (only a miniscule region existed for $s = 9$ TeV). Moreover, as seen before, the left panel in Fig. 11 contains short lines of points in the small m_0-$m_{1/2}$ region with smaller fine tuning than their surrounding points for the same reason as before, namely that $|\mu_{\text{eff}}|$ can be somewhat smaller.

The benchmark point has fine tuning $\Delta_{\text{BM}} = 359$ and $m_h \approx 125$ GeV. The dominance of the $M_{Z'}$ term in Eq. (16) for fine tuning can be seen in the right panel of

Fig. 12, with the familiar dependence on the particular point in the m_0-$m_{1/2}$ plane.

VI. CONCLUSION

Supersymmetric unified models in which the singlet VEV is responsible simultaneously both for μ_{eff} and for the Z' mass, as in the E_6 class of models, for example, have relatively large fine tuning which is typically dominated by the experimental mass limit on the Z'. To illustrate this, we have investigated the degree of fine tuning throughout the parameter space of the cE$_6$SSM. In fact, this is the first time that fine tuning has been studied in any E_6 model containing a TeV scale Z'.

To quantify fine tuning, we have derived a fine-tuning master formula for the E$_6$SSM and implemented it in a spectrum generator for the constrained version of the model. Using this, we scanned the parameter space of the cE$_6$SSM. The results are presented in the m_0-$m_{1/2}$ plane for fixed $\tan\beta = 10$ and various s values corresponding to $M_{Z'} \sim$ 2–4 TeV. This value of $\tan\beta = 10$ is the optimum choice for achieving a large enough Higgs mass in the cE$_6$SSM, and so we have exclusively focused on it here. We selected benchmark points corresponding to each value of s which possess the smallest fine tuning while allowing a Higgs mass within the $124 < m_h < 127$ GeV range, and $m_{\tilde{g}} \geq 850$ GeV. They are the black dot points in Figs. 1–12. These benchmark points and the relevant physical masses are summarized in Table I for a gluino mass of about 900 GeV. Table II shows how the minimum fine tuning changes as the gluino mass limit increases up to 1.5 TeV. As remarked earlier, the fine tuning in the cE$_6$SSM is always significantly smaller than that in the cMSSM, for all gluino masses.

It is clear that the Z' mass (determined by the s VEV value) has a significant effect on the naturalness of the cE$_6$SSM model, with higher values leading to increased fine tuning. Therefore, future improved direct mass limits on the Z' mass from the LHC will imply higher fine tuning. We have also seen an indirect relation between the Higgs boson mass and the Z' mass. For example, if the Higgs mass turns out to be $m_h \gtrsim 127$ GeV, then we are driven to $s \gtrsim 10$ TeV, corresponding to $M_{Z'} \gtrsim 3.8$ TeV, requiring higher fine tuning. Conversely, if the Higgs mass turns out to be $m_h \lesssim 124$ GeV, then $s \gtrsim 5$ TeV, corresponding to $M_{Z'} \gtrsim 1.9$ TeV, allowing lower fine tuning.

Given present limits, the results in Figs. 1–12 and Table I show that the present lowest value of fine tuning in the cE$_6$SSM, consistent with a Higgs mass $m_h \sim 125$ GeV, varies from $\Delta \sim 200$ to 400, where the allowed lowest fine tuning values, taking into account the relevant experimental bounds, are dominated by $M_{Z'}$ rather than the other sources of fine tuning. This is presently significantly lower than the fine tuning in the cMSSM of $\Delta \sim$ 1000 arising from the large stop masses required to achieve the Higgs mass.

In the future, the LHC lower limits on gluino and squark masses will improve, along with the Z' mass limit (or else a discovery will be made), and the Higgs boson mass will be more accurately specified. It is not completely clear where the dominant source of fine tuning in the cE$_6$SSM will originate from in the future. However, the results in this paper allow this question to be addressed. The future Z' mass limit will determine the minimum s value permitted, while the Higgs mass and gluino and squark mass limits will determine the allowed regions of the m_0-$m_{1/2}$ plane, from which the fine tuning may be read off from the contour plots we provide.

ACKNOWLEDGMENTS

We would like to thank Jonathan P. Hall and Kai Schmidt-Hoberg for helpful discussions during early stages of this study. The work of M. B. is funded by King Saud University (Riyadh, Saudi Arabia). S. F. K. acknowledges partial support from the STFC Consolidated ST/J000396/1 and EU ITN Grants UNILHC No. 237920 and INVISIBLES No. 289442. The work of P. A. is supported by the ARC Centre of Excellence for Particle Physics at the Terascale. P. A. would also like to thank Tony Williams for reading the manuscript and offering helpful comments.

APPENDIX A: cE$_6$SSM BENCHMARK POINTS

Table I lists the details on the masses and parameters associated with each benchmark (BM) point that was chosen. We can see that m_0 increases significantly as s ($M_{Z'}$) becomes larger, while $m_{1/2}$ is roughly constant. Upon choosing a BM point, we imposed the limit $m_{1/2} > 1$ TeV to have gluino mass $m_{\tilde{g}} > 850$ GeV. The gluino masses for our benchmark points are about 900 GeV or close to it; hence if the experimental limits on $m_{\tilde{g}}$ are to be increased for constrained models, then fine tuning will increase as well. The lightest stop, $\tilde{t}_1$, masses range from 1.7 to 2.4 TeV for the range of s we studied, and thereby is above the experimental limits.

TABLE I. Parameters and masses for the benchmarks with lowest fine tuning and Higgs masses in the range of $m_h = 124$–125 GeV in the cE$_6$SSM.

	BM1	BM2	BM3	BM4	BM5	BM6
s [TeV]	5	6	7	8	9	10
$\tan\beta$	10	10	10	10	10	10
$\lambda_3(M_X)$	−0.2284	−0.2646	−0.25	−0.2376	−0.2260	−0.2171
$\lambda_{1,2}(M_X)$	0.1	0.1	0.1	0.1	0.1	0.1
$\kappa_{1,2,3}(M_X)$	0.1760	0.1923	0.2111	0.2288	0.2452	0.2601
$m_{1/2}$ [GeV]	1033	1003	1004	1002	1001	1005
m_0 [GeV]	2020	1951	2186	2441	2709	2975
A_0 [GeV]	−83	500	661	781	846	888
$m_{\tilde{D}_1}(1,2,3)$ [GeV]	2252	2234	2659	3149	3680	4222
$m_{\tilde{D}_2}(1,2,3)$ [GeV]	3186	3501	3991	4499	5017	5540
$\mu_D(1,2,3)$ [GeV]	1782	2238	2752	3279	3812	4347
$\lvert m_{\chi_6^0}\rvert$ [GeV]	1973	2349	2727	3105	3483	3861
$m_{h_3} \simeq M_{Z'}$ [GeV]	1889	2267	2645	3023	3401	3779
$\lvert m_{\chi_5^0}\rvert$ [GeV]	1809	2189	2566	2944	3322	3699
$m_s(1,2)$ [GeV]	2448	2548	2897	3263	3639	4014
$m_{H_2}(1,2)$ [GeV]	1970	1847	2023	2218	2426.5	2633
$m_{H_1}(1,2)$ [GeV]	1887	1685	1824	1986	2167	2343
$\mu_{\tilde{H}}(1,2)$ [GeV]	492	569	642	711	777	841
$m_{\tilde{u}_1}(1,2)$ [GeV]	2505	2461	2687	2934	3199	3468
$m_{\tilde{u}_1} \simeq m_{\tilde{d}_1}(1,2)$ [GeV]	2553	2507	2729	2973	3235	3501
$m_{\tilde{d}_2}(1,2)$ [GeV]	2571	2558	2810	3082	3372	3665
$m_{\tilde{e}_1}(1,2,3)$ [GeV]	2136	2107	2366	2641	2935	3224
$m_{\tilde{e}_2}(1,2,3)$ [GeV]	2267	2271	2550	2848	3159	3468
$m_{\tilde{\tau}_1}$ [GeV]	2119	2090	2347	2623	2912	3200
$m_{\tilde{\tau}_2}$ [GeV]	2259	2263	2541	2838	3148	3457
$m_{\tilde{b}_1}$ [GeV]	2202	2151	2340	2549	2777	3009
$m_{\tilde{b}_2}$ [GeV]	2552	2539	2789	3059	3347	3639
$m_{\tilde{t}_1}$ [GeV]	1741	1681	1839	2016	2212	2411
$m_{\tilde{t}_2}$ [GeV]	2215	2166	2354	2561	2787	3018
$\lvert m_{\chi_{3,4}^0}\rvert \simeq \lvert m_{\chi_2^\pm}\rvert$ [GeV]	887	1174	1258	1329	1386	1443
$m_{h_2} \simeq m_A \simeq m_{H^\pm}$ [GeV]	1890	2268	2646	3025	3403	3782
m_h [GeV]	124	124	125	125	125	125
$m_{\tilde{g}}$ [GeV]	901	879	887	892	898	906
$\lvert m_{\chi_1^\pm}\rvert \simeq \lvert m_{\chi_2^0}\rvert$ [GeV]	285	279	279	279	279	280
$\lvert m_{\chi_1^0}\rvert$ [GeV]	162	157	158	158	158	158
$\Delta_{\max}$	251	233	270	302	330	359

APPENDIX B: FINE TUNING AND $m_{\tilde{g}}$

As the lower limits on the gluino mass are expected to rise, Table II shows the minimum amount of the fine tuning corresponding to different values of gluino mass within $m_{\tilde{g}} = 1$–1.5 TeV, and for $s = 5$–10 TeV. The corresponding Higgs mass is shown in parentheses next to each value of fine tuning.

TABLE II. For different values of the singlet VEV ($s = 5$–10 TeV) corresponding to $M_{Z'} \sim 2$–3.8 TeV, the effect of raising the lower limit on the gluino mass between $m_{\tilde{g}} = 1$ and 1.5 TeV on fine tuning is shown. Next to every fine-tuning value, the corresponding Higgs mass (in GeV) is shown between parentheses. An empty cell [$\cdots$] means that no $m_h \sim 124$–127 GeV is found in the scanned parameter space.

s [TeV]	5	6	7	8	9	10
$m_{\tilde{g}}$ [TeV]			Δ (m_h [GeV])			
1	293 (124)	297 (124)	324 (125)	367 (125)	405 (126)	443 (126)
1.1	388 (125)	348 (124)	358 (124)	408 (125)	454 (126)	497 (126)
1.2	474 (124)	440 (125)	400 (124)	448 (125)	500 (126)	550 (126)
1.3	$\cdots$	556 (125)	462 (124)	484 (124)	547 (126)	600 (126)
1.4	$\cdots$	658 (125)	617 (126)	525 (124)	587 (125)	650 (126)
1.5	$\cdots$	$\cdots$	767 (125)	635 (125)	628 (125)	699 (126)

[1] G. Aad *et al.* (ATLAS Collaboration), J. High Energy Phys. 11 (2012) 094.
[2] G. Aad *et al.* (ATLAS Collaboration), J. High Energy Phys. 07 (2012) 167.
[3] G. Aad *et al.* (ATLAS Collaboration), Phys. Lett. B **716**, 1 (2012).
[4] S. Chatrchyan *et al.* (CMS Collaboration), Phys. Lett. B **716**, 30 (2012).
[5] D. J. H. Chung, L. L. Everett, G. L. Kane, S. F. King, J. D. Lykken, and L.-T. Wang, Phys. Rep. **407**, 1 (2005).
[6] S. Cassel and D. M. Ghilencea, Mod. Phys. Lett. A **27**, 1230003 (2012).
[7] D. M. Ghilencea, H. M. Lee, and M. Park, J. High Energy Phys. 07 (2012) 046.
[8] S. F. King, S. Moretti, and R. Nevzorov, Phys. Rev. D **73**, 035009 (2006).
[9] S. F. King, S. Moretti, and R. Nevzorov, Phys. Lett. B **634**, 278 (2006).
[10] U. Ellwanger, M. Rausch de Traubenberg, and C. A. Savoy, Phys. Lett. B **315**, 331 (1993); Z. Phys. C **67**, 665 (1995); Nucl. Phys. **B492**, 21 (1997); U. Ellwanger, Phys. Lett. B **303**, 271 (1993); P. Pandita, Z. Phys. C **59**, 575 (1993); T. Elliott, S. F. King, and P. L. White, Phys. Rev. D **49**, 2435 (1994); S. F. King and P. L. White, Phys. Rev. D **52**, 4183 (1995); F. Franke and H. Fraas, Int. J. Mod. Phys. A **12**, 479 (1997).
[11] S. Chatrchyan *et al.* (CMS Collaboration), Phys. Lett. B **714**, 158 (2012).
[12] P. Athron, S. F. King, D. J. Miller, S. Moretti, and R. Nevzorov, Phys. Rev. D **84**, 055006 (2011).
[13] P. Athron, J. P. Hall, R. Howl, S. F. King, D. J. Miller, S. Moretti, and R. Nevzorov, Nucl. Phys. B, Proc. Suppl. **200–202**, 120 (2010).
[14] P. Athron, S. F. King, D. J. Miller, S. Moretti, and R. Nevzorov, Phys. Rev. D **80**, 035009 (2009).
[15] P. Athron, S. F. King, D. J. Miller, S. Moretti, and R. Nevzorov, Phys. Lett. B **681**, 448 (2009).
[16] P. Athron, S. F. King, D. J. Miller, S. Moretti, and R. Nevzorov, Phys. Rev. D **86**, 095003 (2012).
[17] P. Athron, D. Stockinger, and A. Voigt, Phys. Rev. D **86**, 095012 (2012).
[18] J. C. Callaghan and S. F. King, J. High Energy Phys. 04 (2013) 034.
[19] R. Howl and S. F. King, J. High Energy Phys. 05 (2008) 008.
[20] R. Howl and S. F. King, Phys. Lett. B **687**, 355 (2010).
[21] J. R. Ellis, K. Enqvist, D. V. Nanopoulos, and F. Zwirner, Mod. Phys. Lett. A **01**, 57 (1986).
[22] R. Barbieri and G. F. Giudice, Nucl. Phys. **B306**, 63 (1988).
[23] B. de Carlos and J. A. Casas, Phys. Lett. B **309**, 320 (1993).
[24] B. de Carlos and J. A. Casas, arXiv:hep-ph/9310232.
[25] P. H. Chankowski, J. R. Ellis, and S. Pokorski, Phys. Lett. B **423**, 327 (1998).
[26] K. Agashe and M. Graesser, Nucl. Phys. **B507**, 3 (1997).
[27] D. Wright, arXiv:hep-ph/9801449.
[28] G. L. Kane and S. F. King, Phys. Lett. B **451**, 113 (1999).
[29] M. Bastero-Gil, G. L. Kane, and S. F. King, Phys. Lett. B **474**, 103 (2000).
[30] J. L. Feng, K. T. Matchev, and T. Moroi, Phys. Rev. D **61**, 075005 (2000).
[31] B. C. Allanach, J. P. J. Hetherington, M. A. Parker, and B. R. Webber, J. High Energy Phys. 08 (2000) 017.
[32] B. C. Allanach, Phys. Lett. B **635**, 123 (2006).

[33] T. Kobayashi, H. Terao, and A. Tsuchiya, Phys. Rev. D **74**, 015002 (2006).
[34] R. Dermisek and J. F. Gunion, Phys. Rev. Lett. **95**, 041801 (2005).
[35] R. Barbieri and L. J. Hall, arXiv:hep-ph/0510243.
[36] R. Barbieri, L. J. Hall, and V. S. Rychkov, Phys. Rev. D **74**, 015007 (2006).
[37] B. Gripaios and S. M. West, Phys. Rev. D **74**, 075002 (2006).
[38] R. Dermisek, J. F. Gunion, and B. McElrath, Phys. Rev. D **76**, 051105 (2007).
[39] M. Perelstein and B. Shakya, arXiv:1208.0833.
[40] S. Antusch, L. Calibbi, V. Maurer, M. Monaco, and M. Spinrath, J. High Energy Phys. 01 (2013) 187.
[41] T. Cheng, J. Li, T. Li, X. Wan, Y. k. Wang, and S.-h. Zhu, arXiv:1207.6392.
[42] M. W. Cahill-Rowley, J. L. Hewett, A. Ismail, and T. G. Rizzo, Phys. Rev. D **86**, 075015 (2012).
[43] G. G. Ross, K. Schmidt-Hoberg, and F. Staub, J. High Energy Phys. 08 (2012) 074.
[44] T. Basak and S. Mohanty, Phys. Rev. D **86**, 075031 (2012).
[45] Z. Kang, J. Li, and T. Li, J. High Energy Phys. 11 (2012) 024.
[46] G. W. Anderson and D. J. Castano, Phys. Lett. B **347**, 300 (1995).
[47] G. W. Anderson and D. J. Castano, Phys. Rev. D **52**, 1693 (1995).
[48] G. W. Anderson and D. J. Castano, Phys. Rev. D **53**, 2403 (1996).
[49] G. W. Anderson, D. J. Castano, and A. Riotto, Phys. Rev. D **55**, 2950 (1997).
[50] P. Ciafaloni and A. Strumia, Nucl. Phys. **B494**, 41 (1997).
[51] K. L. Chan, U. Chattopadhyay, and P. Nath, Phys. Rev. D **58**, 096004 (1998).
[52] R. Barbieri and A. Strumia, Phys. Lett. B **433**, 63 (1998).
[53] L. Giusti, A. Romanino, and A. Strumia, Nucl. Phys. **B550**, 3 (1999).
[54] J. A. Casas, J. R. Espinosa, and I. Hidalgo, J. High Energy Phys. 01 (2004) 008.
[55] J. A. Casas, J. R. Espinosa, and I. Hidalgo, arXiv:hep-ph/0402017.
[56] J. A. Casas, J. R. Espinosa, and I. Hidalgo, J. High Energy Phys. 11 (2004) 057.
[57] J. A. Casas, J. R. Espinosa, and I. Hidalgo, Nucl. Phys. **B777**, 226 (2007).
[58] R. Kitano and Y. Nomura, Phys. Lett. B **631**, 58 (2005).
[59] P. Athron and D. J. Miller, Phys. Rev. D **76**, 075010 (2007).
[60] H. Baer, V. Barger, P. Huang, A. Mustafayev, and X. Tata, Phys. Rev. Lett. **109**, 161802 (2012).
[61] B. C. Allanach, K. Cranmer, C. G. Lester, and A. M. Weber, J. High Energy Phys. 08 (2007) 023.
[62] M. E. Cabrera, J. A. Casas, and R. Ruiz de Austri, J. High Energy Phys. 03 (2009) 075.
[63] D. M. Ghilencea and G. G. Ross, Nucl. Phys. **B868**, 65 (2013).
[64] S. Fichet, Phys. Rev. D **86**, 125029 (2012).
[65] M. E. Cabrera, J. A. Casas, and R. Ruiz de Austri, J. High Energy Phys. 05 (2010) 043.
[66] C. Balazs, A. Buckley, D. Carter, B. Farmer, and M. White, arXiv:1205.1568.
[67] A. Belyaev, J. P. Hall, S. F. King, and P. Svantesson, Phys. Rev. D **86**, 031702 (2012); **87**, 035019 (2013).